

Original Article

Cite this article: Baba S, Owada M, Hokada T, Adachi T, and Nakano N (2023) Contrasting geological background based on the geochemistry of the mafic metamorphic rocks in central Dronning Maud Land. *Geological Magazine* **160**: 993–1009. <https://doi.org/10.1017/S0016756823000092>

Received: 26 September 2022
Revised: 11 January 2023
Accepted: 2 February 2023
First published online: 20 March 2023


Keywords:

East Antarctica; Dronning Maud Land; geochemistry; tectonic setting

Author for correspondence:

Sotaro Baba,
Email: baba@edu.u-ryukyu.ac.jp

Contrasting geological background based on the geochemistry of the mafic metamorphic rocks in central Dronning Maud Land

Sotaro Baba¹ , Masaaki Owada², Tomokazu Hokada³, Tatsuro Adachi⁴ and Nobuhiko Nakano⁴

¹Department of Science Education, University of the Ryukyus, Okinawa 903-0213, Japan; ²Department of Earth Sciences, Yamaguchi University, Yamaguchi, 753-8512 Japan; ³National Institute of Polar Research, Tokyo 190-8518, Japan and ⁴Division of Earth Sciences, Faculty of Social and Cultural Studies, Kyushu University, Fukuoka 819-0395, Japan

Abstract

This paper reports geochemical characteristics of mafic gneisses and granulites collected from four localities in central Dronning Maud Land to evaluate the tectonic setting of their precursor rocks. Precursor rocks for the mafic gneisses and granulites in central Dronning Maud Land were formed in different geological backgrounds and tectonic settings. The mafic gneisses and granulites in the Schirmacher Hills were derived from basaltic rocks in a back-arc setting. Published U–Pb zircon ages and the geochemical variation of the basement rocks indicate their emplacement between 800 and 650 Ma, close to peak metamorphism. While similar protoliths were recognized in the inland nunataks of Hochlinfjellet, in Filchnerfjella the mafic gneisses/granulites were derived from basaltic rocks formed in marginal continental arcs or island arcs. Highly disturbed trace-element patterns indicate that the metamorphic process influenced the geochemical composition during the prograde metamorphic stage. Our results imply that the outcrops in central Dronning Maud Land with different metamorphic ages contain mafic gneisses/granulites from precursor rocks formed under different tectonic settings.

1. Introduction

Understanding the evolutionary history of orogenic belts is crucial to revealing the continental growth of the active Earth. Geochemical data contribute to the estimation of the geological background and provinces of orogenic belts. The formation of the Gondwana supercontinent was a global event that resulted in the formation of widespread orogenic belts, including the East Africa–Antarctica Orogen (EAAO) (Fig. 1a; Jacobs & Thomas, 2004) at 650–500 Ma, or two separate East Africa Orogen (EAO) events (Stern, 1994) at 650 ± 50 Ma and the subsequent Kuunga Orogeny at 550 ± 50 Ma (Meert, 2003; Grantham *et al.* 2008). The orogenic belt extends more than 8000 km and acts as the collision zone between East and West Gondwana.

The mountain range of central Dronning Maud Land (DML) is sub-parallel to and 200–250 km inland from the edge of the East Antarctica ice sheet (Fig. 1a). Central DML occupies the core part of the past EAAO or EAO and Kuunga Orogeny. The main collisional event in central DML was in the range of the Kuunga Orogeny (e.g. Pan-African I at c. 560–550 Ma and Pan-African II at c. 530–490 Ma; Jacobs *et al.* 2003). Zircon U–Pb age data obtained from metamorphic rocks from several localities in central DML have revealed different timings of metamorphism at c. 640 Ma, 600 Ma and 520 Ma (Baba *et al.* 2010, 2015). Therefore, the older EAO event of 650 ± 50 Ma extends to the Antarctic region.

Grantham *et al.* (2008, 2013) proposed a megathrust tectonic model forming meganappe/klippen for the geological evolution of central and eastern DML. Grantham *et al.* (2008) pointed out that the Schirmacher Hills have ages comparable with those of the Namuno terrane and klippen (Mugeba and Monapo complexes) in northern Mozambique (Fig. 1). Still, the distinctive ultra-high temperature (UHT) metamorphism in the Schirmacher Hills (Baba *et al.* 2006, 2010) has not been detected in these localities. The Nampula terrane in southern Mozambique, the footwall of the megathrust, which is equivalent to central DML (Grantham *et al.* 2013), does not preserve 640 Ma and 600 Ma metamorphic events. In addition, c. 800 Ma magmatism dated from the Schirmacher Hills is limited to several localities in the Namuno terrane (Bingen *et al.* 2009) and needs to be better detected in these klippen.

Baba *et al.* (2015) have proposed a preliminary terrane division based on the protolith age and the timing of metamorphism in central DML (Fig. 1b). However, the interrelationships and tectonic settings of the different metamorphic ages are not fully understood. Jacobs *et al.* (2015, 2017) proposed two basement provinces in central to eastern DML: the Grenville-aged Maud Belt and the Tonian Oceanic Arc Super Terrane (TOAST) (Fig. 1a). According to their models,

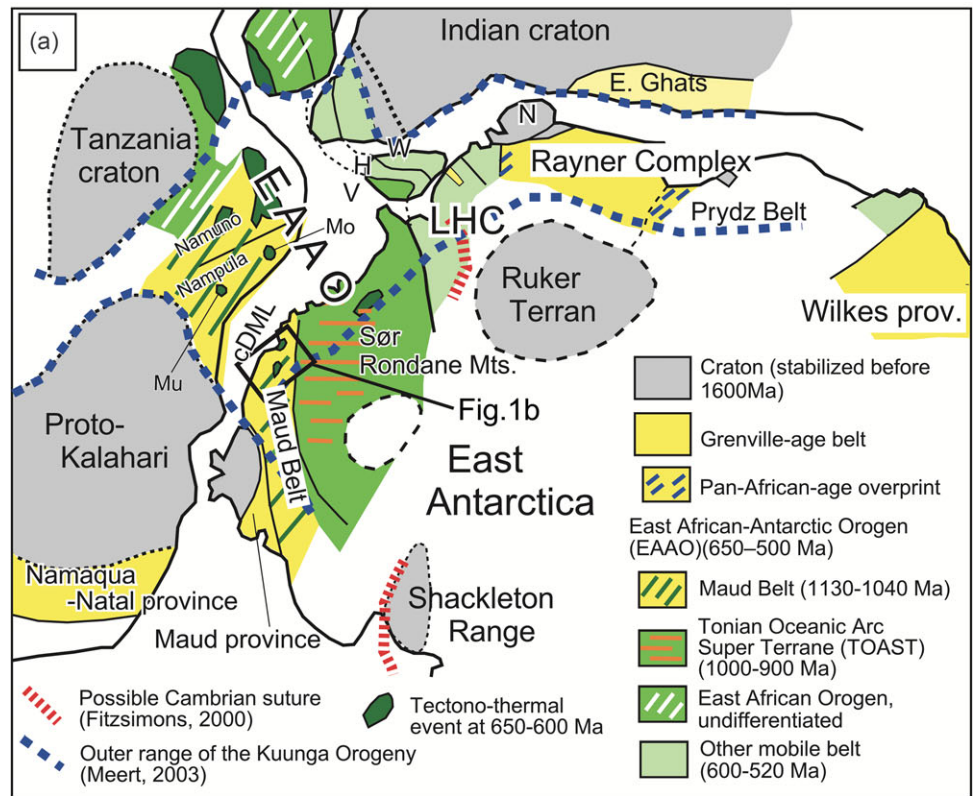
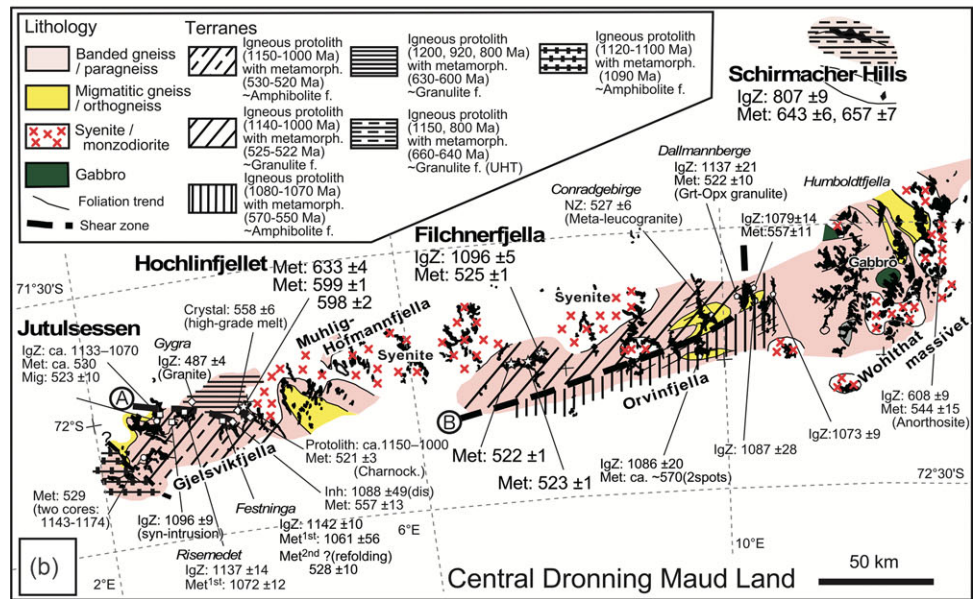


Fig. 1. (Colour online) (a) Reconstruction of East Antarctica and adjacent parts of Gondwana at 500 Ma (after Fitzsimons, 2000; Shiraishi *et al.* 2008; Grantham *et al.* 2013; Jacobs *et al.* 2015; Ruppel *et al.* 2018). The Lützow-Holm Complex (LHC) is situated adjacent to the East African–Antarctic Orogen (EAAO). Key sutures and orogenic belts are taken from Fitzsimons (2000) and Meert (2003). Abbreviations: H – Highland Complex; N – Napier Complex; V – Vijayan Complex; W – Wannai Complex; cDML – central Dronning Maud Land; Mo – Monapo Complex; Mu – Mugeba Complex. (b) Map showing study area and preliminary terrane division of central Dronning Maud Land. Published U–Pb ages obtained by SHRIMP and secondary ion mass spectrometry (SIMS) are also shown (after Baba *et al.* 2015 and references therein). Dashed lines A and B represent possible terrane boundary. Abbreviations: Crystal – crystallization age from melt; dis – discordia age; f. – facies; Grt–Opx – garnet–orthopyroxene; IgZ – igneous zircon; Inh – inherited; Met – timing of peak metamorphism; Metamorph. – metamorphism; Mig – timing of migmatization; NZ – newly crystallized zircon; UHT – ultra-high temperature.



central DML belongs to the Grenville-aged Maud Belt, which has older protolith ages ranging from 1130 to 1040 Ma, with metamorphic overprints at 600 Ma, 570–550 Ma and 530–515 Ma. The TOAST represents juvenile subduction-related oceanic arcs ranging from 1000 to 900 Ma. Therefore, the simple collision of the two vast continents, East and West Gondwana, is now debatable, considering presence of the TOAST.

Previous studies have reported many ages from central to eastern DML; however, there is little information about the tectonic setting of the precursors of the metamorphic rocks. This study reveals the tectonic setting of the mafic metamorphic rocks

of four localities in central DML based on their geochemistry and previously published age data.

2. Geological setting

The central DML nunataks consist of high-grade metamorphic rocks and a series of post-tectonic igneous rocks. The metamorphic rocks are banded gneisses associated with supracrustal components and migmatites of various compositions that have been metamorphosed under amphibolite- to granulite-facies conditions. The igneous rocks are mainly A-type granitoids, and they

are exposed over a large area from Sverdrupfjella in the west to Wohlthatmassivet in the east (Fig. 1b). They are considered to have formed owing to the melting of an over-thickened crust derived from the collision of East and West Gondwana during the Pan-African orogeny in the late Neoproterozoic to early Palaeozoic era (Jacobs *et al.* 2003). The older Mesoproterozoic (c. 1.1 Ga) rocks in central DML were reworked during the early Palaeozoic era with intense reworking in central DML as compared to those of western DML (e.g. Heimefrontfjella and Kirwanveggen).

2.a. Schirmacher Hills

The Schirmacher Hills (11° 20'–11° 55' E, 70° 45' S) are an isolated exposure on the Princess Astrid coast in central DML. The high-grade metamorphic rocks are divided into the following units (Fig. 2a): (1) quartzo-feldspathic gneiss, (2) augen gneiss, (3) a mixed zone including metapelite and calc-silicate gneiss, mafic granulite and charnockite, (4) garnet-biotite gneiss, and (5) banded gneiss (Sengupta, 1993; Rameshwar Rao *et al.* 1997).

The banded gneiss unit is predominantly composed of biotite-hornblende or biotite gneiss with a smaller fraction of garnet-bearing gneiss, mafic to intermediate granulite, garnet-amphibolite, garnet-rich biotite gneiss and pyroxenite. The mafic granulite has variable amounts of garnet, clinopyroxene and orthopyroxene and occurs as discontinuous layers and blocks. Highly deformed gneisses occur locally. The analysed mafic granulites and gneisses originated from the banded gneiss unit in the eastern part of the Schirmacher Hills (Fig. 2a).

2.b. Hochlinfjellet

Hochlinfjellet (72° 05' S, 4° 03' E) is located in the western part of the Mühlig–Hofmannfjella (72° 00'–72° 05' S, 3° 50'–5° 30' E) (Fig. 2b). A regional geological map of this region was published by Ohta (1993). This area consists mainly of banded gneiss and migmatized biotite-hornblende schist/gneiss (Paulsson & Austrheim, 2003; Bucher & Frost, 2006) (Fig. 2b). The banded gneisses include layered micaceous gneisses, marbles, calc-silicate rocks, garnet-sillimanite gneisses, quartzo-feldspathic gneisses, amphibolites and metamorphosed basic dykes, which predominate west of the Hochlinfjellet nunataks. They were deformed and locally migmatized to various degrees. Post-tectonic intrusions of A-type granitoids, syenite, occur extensively in the nunataks between Hochlinfjellet and Filchnerfjella.

2.c. Jutulsessen

Jutulsessen is located in the central portion of Gjelsvikfjella (2° 30'–2° 50' E, 72° 00'–72° 05' S). The geology of this region (Fig. 2c) is identical to that of Hochlinfjellet (Ohta, 1993). Investigation near Troll Station showed the presence of garnet-sillimanite-bearing pelitic gneiss and garnet-clinopyroxene-, garnet-hornblende- and garnet-orthopyroxene-bearing mafic gneisses. All samples were collected near Troll Station.

2.d. Filchnerfjella

Filchnerfjella (Fig. 2d) is located near the eastern edge of the Mühlig–Hofmannfjella and is underlain by granulite-facies metamorphic rocks that are intruded by a series of post-tectonic charnockite, syenite, quartz-syenite, granite and several generations of

dykes (Owada *et al.* 2003, 2008; Engvik & Elvevold, 2004). The metamorphic rocks are divided into three units (Fig. 2d): (1) garnet-bearing leucocratic gneisses (leucogneiss unit); (2) orthopyroxene-bearing brown gneisses with dark-coloured feldspars (brown gneiss unit); and (3) variably coloured and layered gneisses comprising alternating layers of gneiss associated with rock units of (1) and (2) (layered gneiss unit; Owada *et al.* 2003). The detailed lithological composition of each unit is described in Baba *et al.* (2015). Mafic gneisses with various mineral assemblages of garnet-clinopyroxene-hornblende, garnet-hornblende, two-pyroxene and garnet-orthopyroxene-hornblende were collected for analysis.

2.e. Metamorphism and age relationships

The metamorphic pressure–temperature (*P–T*) paths of the studied regions commonly show a clockwise trajectory (Baba *et al.* 2015). An isothermal decompression retrograde path characterizes the inland nunataks of Filchnerfjella, Jutulsessen and Hochlinfjellet, as evidenced by the corona texture of orthopyroxene symplectite and plagioclase replacing garnet (Owada *et al.* 2003; Baba *et al.* 2008). Cordierites replacing garnet and sillimanite in the pelitic gneisses from Filchnerfjella and Hochlinfjellet also indicate a history of decompression metamorphism. U–Pb zircon age data show two separate metamorphism stages, at 630–600 Ma for Hochlinfjellet and 520 Ma for Filchnerfjella. Since zircons with texturally similar internal domains were analysed, they were interpreted to have formed close to the peak metamorphism, and not during the prolonged retrograde cooling phase (Elvevold *et al.* 2020).

The coastal outcrop of Schirmacher Hills recorded UHT conditions with a clockwise *P–T* path involving an isobaric cooling (IBC) retrograde history (Baba *et al.* 2006, 2010) in marked contrast to those of the inland nunataks. Garnet-bearing mafic granulite exhibits tiny garnet grains formed on large plagioclase grains, clinopyroxene and quartz (Baba *et al.* 2008). Garnet coronae developed around orthopyroxene and ilmenite also suggest an IBC history. The U–Pb zircon age for this coastal outcrop reveals UHT metamorphism occurring at 660–640 Ma, which is older than that of the inland nunataks. Jacobs *et al.* (2020) reported similar metamorphic ages older than 600 Ma from the other lithologies in the Schirmacher Hills and neighbouring exposures.

3. Analytical methods

To determine the bulk whole-rock chemical compositions of the 47 samples, rock slabs of each sample, c. 10 × 10 × 3 cm, were selected to avoid local exotic veins. The samples were ground in a stainless steel mortar to ~2 mm, and divided by coning and quartering to obtain a 25 g aliquot, which was then pulverized in a quartz ball mill using a FRITSCH Pulverisette 6. Before fusion, all powdered samples were heated at 900 °C for 2.5 h to remove volatiles and oxidize the ferrous iron. These samples were carefully weighed at 1.0000 ± 0.0005 g, thoroughly mixed with 5× excess Li-metaborate, and fused to form a glass bead in an induction furnace using a TK-4200 Bead Sampler (Tokyo-Kagaku Co., Ltd) by heating in several stages: first at 800 °C for 2 min, then at 1200 °C for 2.5 min and, finally, swing heating at 1200 °C for 3 min. The whole-rock element contents were determined using a SHIMAZU-1800 X-ray fluorescence (XRF) spectrometer instrument at the University of the Ryukyus, equipped with a Rh-tube operated at 60 kV and 50 mA. The XRF analytical procedure described by

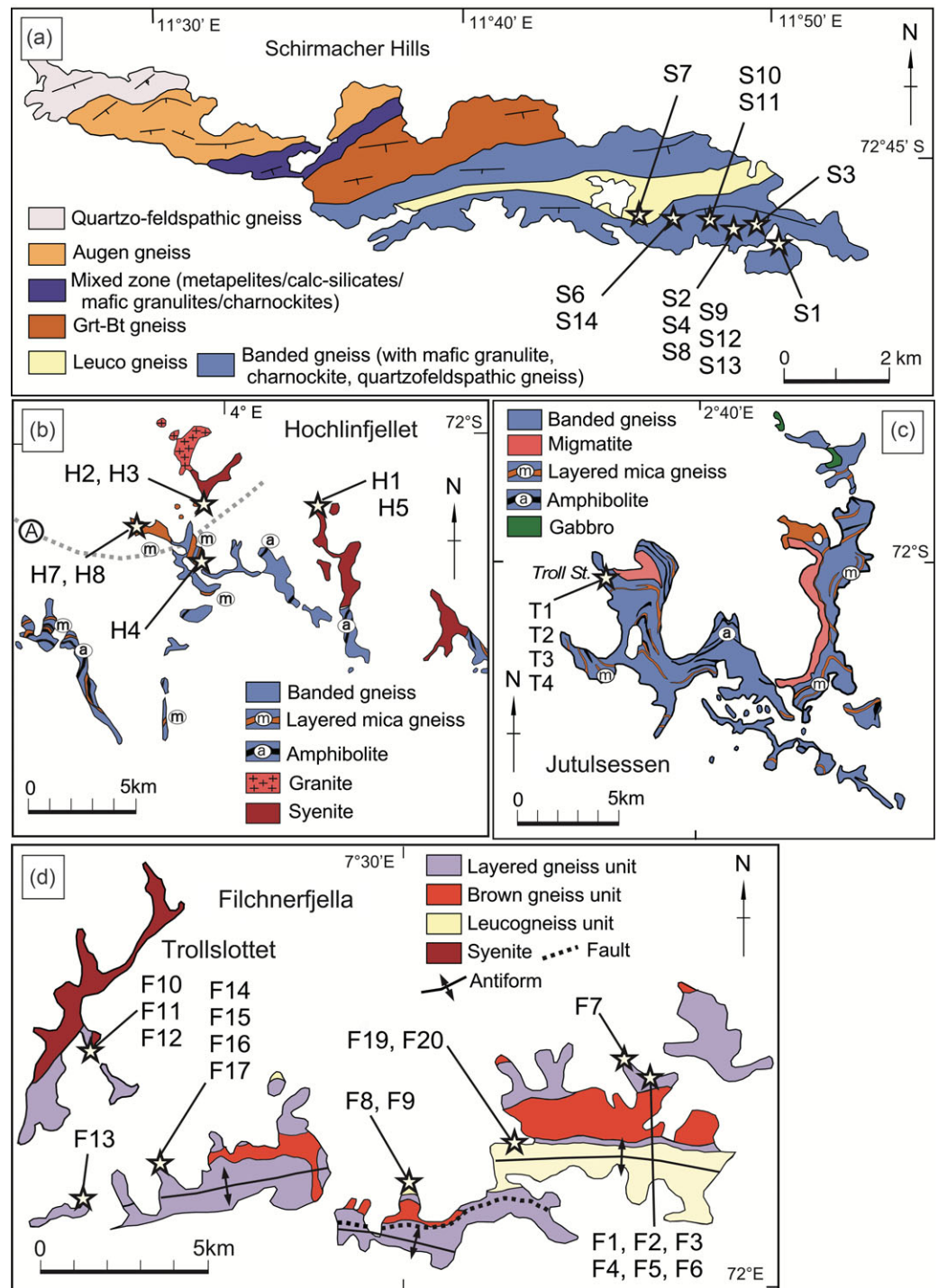


Fig. 2. (Colour online) Simplified geological map of the study area showing the sample localities. (a) Schirmacher Hills (modified after Sengupta, 1993; Rameshwar Rao *et al.* 1997); (b) Hochlinfjellet and (c) Jutulsessen (modified after Ohta, 1993); (d) Filchnerfjella (Owada *et al.* 2003).

Shinjo & Miyamoto (2007) was followed. Raw X-ray intensities were converted to concentrations using a calibration curve that was prepared using 14 natural and synthetic standards. The theoretical coefficients for the matrix correction were calibrated using the attached standard software (PCXRF ver. 1.11).

Trace and rare earth elements (REEs) of 36 selected samples were analysed by inductively coupled plasma mass spectrometry (ICP-MS) and by instrumental neutron activation analysis (INAA) at Activation Laboratories, Canada (code 4B2-research + 4BINAA).

4. Sample description

A total of 47 mafic gneisses from central DML were selected for analysis (Fig. 3a, b, e, f). Table 1 lists the mineral assemblages of the analysed mafic gneisses. The mafic gneisses have various assemblages: hornblende, clinopyroxene, orthopyroxene, garnet, plagioclase, quartz, secondary biotite and cummingtonite with accessory minerals of Fe-Ti oxides, apatite, titanite and calcite (Fig. 3c, d, g, h). There were slight differences in the abundance and occurrence of the constituent minerals among the sampling areas.

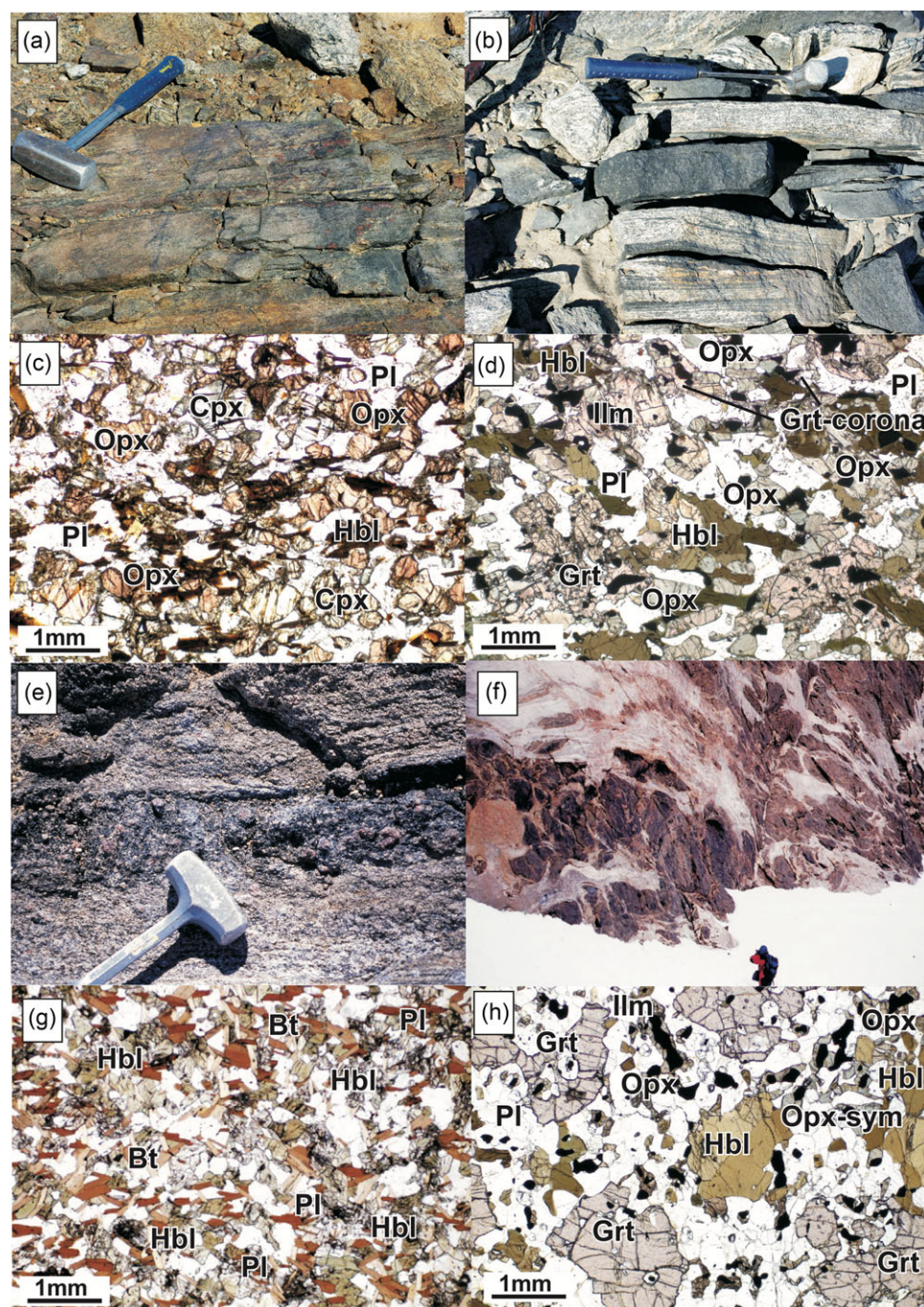


Fig. 3. (Colour online) Occurrences of mafic granulite/gneiss and photomicrographs of analysed rocks. (a, b) Mafic granulite/gneiss layers occurring concordantly with host felsic gneisses in the Schirmacher Hills. (c, d) Photomicrographs of samples S5 and S8. (e) Mafic granulite occurring as a continuous layer in the layered gneiss unit in Filchnerfjella. (f) Mafic gneiss blocks in the leucogneiss unit in Filchnerfjella. (g, h) Photomicrographs of samples F9 and F18. Length of the hammer for scale is 12 cm.

In Filchnerfjella, mafic gneisses mainly consist of hornblende, orthopyroxene, biotite, plagioclase and quartz, and are occasionally associated with garnet or clinopyroxene. Orthopyroxene occurs as fine grains between garnet and hornblende and sometimes occurs as symplectite with plagioclase and coronae around the ilmenite. Garnets and clinopyroxene were not detected in the same sample. Detailed petrographic descriptions of the mafic rocks in Filchnerfjella have been presented by Owada *et al.* (2003).

In the Schirmacher Hills, garnet, orthopyroxene and biotite dominate the mafic gneisses/granulites, and hornblende and

clinopyroxene are subordinate. Cummingtonite occurs as a secondary mineral, replacing orthopyroxene and clinopyroxene in many samples. Most garnet occurs as irregularly shaped grains and sometimes as coronae around the ilmenite and orthopyroxene.

Samples from Jutulsessen lack the orthopyroxene–clinopyroxene association. However, orthopyroxene symplectite develops; replacement of garnet and hornblende is similar to Filchnerfjella. In Hochlinfjellet, garnet–clinopyroxene-bearing mafic rocks are rare, but orthopyroxene symplectite was observed in one sample (Baba *et al.* 2008).

Table 1. Relative mineral abundances of analysed samples

Sample no.	ID no.	Assemblage	Mafic: Felsic	Pl	Qtz	Hbl	Bt	Opx	Cpx	Grt	Cum	Trace	Note	SiO ₂
Filchnerfjella														(wt %)
02010202B	F1	Two Px	50:50	80	20	-	++ +	++	++	n	n	Ap		51.7
02010202F	F2	Cpx-Hbl	100:0	-	-	++	+	n	++ +	n	n	Ilm		43.4
02010202G	F3	Cpx-Hbl	100:0	-	-	++	+	+	++ +	n	n	Ilm		45.5
02010202H	F4	Two Px	70:30	50	50	++ +	+	++	++	n	n	Ap	Qtz-rich	56.9
02010202I	F5	Hbl-Opx	70:30	50	50	++ +	-	++ +	n	n	n			51.0
02010202J	F6	Hbl-Opx	50:50	70	30	++ +	++	+	n	n	n	Ap, Hem		47.5
02010203B	F7	Opx-Bt	50:50	80	20	n	++ +	++ +	-	n	n	Ap	Myrmekite	49.0
02010301I	F8	Hbl-Bt	50:50	70	30	++ +	++ +	-	n	n	n	Ilm, Ap		54.6
02010301J	F9	Hbl-Bt	50:50	50	50	++ +	++ +	-	n	n	n	Ap	Opx->Hbl?	47.6
02010401B	F10	Hbl-Bt	50:50	80	20	++ +	++ +	++	n	n	n	Hem		56.2
02010401C	F11	Two Px	50:50	80	20	+	++	++ +	++	n	n	Ap		49.0
02010401D	F12	Two Px	50:50	80	20	++	++	++	++	n	n	Ap		55.8
02010502H	F13	Two Px	60:40	70	30	++ +	++ +	++	++	n	n	Ilm		45.3
02010601A	F14	Hbl-Opx	70:30	70	30	++	++	++	++	n	n			43.0
02010601B	F15	Grt-Opx-Hbl	70:30	80	20	++ +	+	++	n	++ +	n	Spl, Ilm	Opx sym.	42.2
02010601G	F18	Grt-Opx-Hbl	50:50	80	20	++	+	++	n	++ +	n	Ilm		39.4
02010701A	F21	Opx-Bt	50:50	80	20	+	++ +	++ +	-	n	n	Ap, Zrn		60.9
02010601D	F10	Grt-Opx-Hbl	70:30	70	30	++ +	n	+	n	++	n	Ap, Ilm		44.4
02010601F	F17	Hbl-Opx	50:50	70	30	++ +	n	++	n	n	n	Ap		47.6
02010602A	F19	Grt-Opx-Hbl	50:50	70	30	++ +	+	++ +	n	++	n	Ilm, Ap	Poikilitic Pl	41.5
02010602B	F20	Hbl-Opx	50:50	70	30	++ +	++	+	n	n	n	Ap		49.3
Hochlinfjellet														
B01122102A	H7	Hbl-Opx	30:70	70	30	++ +	n	+	n	n	n	Ilm		50.2
B01122109	H8	Hbl-Opx	70:30	70	30	++ +	-	++ +	n	n	n	Ilm	Opx sym.	46.5
01120T01C	H1	Hbl-Opx	30:70	80	20	++ +	+	++	n	n	n	Ap		49.7
01121901A	H2	Hbl-Bt	50:50	70	30	++ +	++	n	n	n	n	Ilm, Ap		48.2
01121901C	H3	Hbl-Bt	50:50	80	20	++	++	n	n	n	n	Ilm, Ap		46.7

(Continued)

Table 1. (Continued)

Sample no.	ID no.	Assemblage	Mafic: Felsic	Pl	Qtz	Hbl	Bt	Opx	Cpx	Grt	Cum	Trace	Note	SiO ₂
01121902A	H4	Hbl-Bt	50:50	80	20	++ +	+	n	n	n	n	Ap		48.9
01122002C	H5	Hbl-Bt	50:50	80	20	++ +	+	n	n	n	n	Ap, Ilm		42.8
Jutulsessen														
Troll 2	T1	Grt-Opx	70:30	70	30	++ +	+	++ +	n	++	n	Ilm	Opx sym.	42.9
Troll3	T2	Grt-Opx	50:50	50	50	++ +	-	++	n	-	n	Ilm, Ap		46.3
Troll4	T3	Hbl-Bt	50:50	50	50	++ +	++ +	n	n	n	n	Ilm, Ap		43.5
Troll5	T4	Grt-Cpx	50:50	50	50	++	-	n	++	++ +	n	Ilm		45.1
Schirmacher Hills														
08020401H	S1	Grt-Opx	50:50	70	30	n	+	++	n	++	-	Ilm, Ap		47.9
08020402'	S3	Hbl	80:20	100	0	++ +	+	n	n	n	++	Ilm, Ap	Green & brown Hbl	45.8
08020404C	S2	Grt-Opx	60:40	90	10	n	++	++	n	++ +	n	Ilm, Ap		46.6
08020404D	S4	Opx-Cum	50:50	100	0	n	++	++	n	n	++ +	Ilm, Ap	Sec. Cum	49.8
08020404F	S12	Grt-Bt	60:40	70	30	n	++	n	n	++ +	n	Ilm, Ap		40.4
08020404G	S8	Grt-Opx	50:50	90	10	++	n	++ +	+	++	++	Ilm, Ap	Grt corona	43.8
08020404H	S13	Grt-Bt	60:40	70	30	n	++	n	n	++ +	n	Ilm, Ap		38.8
08020404J	S9	Grt-Cpx-Hbl	70:30	90	10	++ +	-	+	++	++	+	Ilm, Ap		41.8
08020405B	S10	Grt-Cpx	80:20	90	10	+	+	n	++	++ +	++ +	Ilm, Ap	Grt corona	50.5
08020405C	S11	Grt-Opx	50:50	80	20	-	-	++ +	++	++	n	Ilm, Ap		45.9
08020406A	S6	Two Px	50:60	100	0	++	n	++	++	n	n	Ilm, Ap		47.0
08020406B	S14	Grt-Opx	90:10	90	10	++	++	+	+	++	++	Ilm, Ap	Grt corona	39.8
08020407	S7	Cum-Bt	70:30	90	10	+	++	n	n	n	++ +	Ilm, Ap		49.0

Sym - symplectite; Sec - secondary; abundance: +++ > ++ > + > -; n - not present.

5. Results

The chemical compositions of the mafic gneisses/granulites are listed in Table 2 and online Supplementary Material Table S1. The Mg number versus SiO₂/Al₂O₃ diagram (Kempton & Harmon, 1992; Kempton *et al.* 1997) for the mafic gneisses in central DML is shown in Figure 4. In general, the progress of magmatic differentiation and the accumulation of Fe-Ti oxides causes a decrease in the Mg number. The SiO₂/Al₂O₃ ratios reflect the magmatic fractionation series: alkalic, tholeiitic and calc-alkaline. These ratios increase with pyroxene accumulation and decrease with plagioclase accumulation. Primitive basaltic magmas plot in a narrow field, as shown in Figure 4 (Kempton *et al.* 1997).

These data around the primitive basaltic magmas within a range of Mg no. = 42–70 and SiO₂/Al₂O₃ = 2.5–5.0, represented as a dashed solid line, are used in subsequent discrimination diagrams in the later discussion.

The normal mid-ocean ridge basalt (N-MORB)-normalized trace-element patterns and chondrite-normalized REE element patterns for the analysed samples are shown in Figures 5 and 6. The compositional data range of SiO₂ is from 42 to 52 wt %. The grey lines represent the data belonging to the ultra-basic compositions (SiO₂ = 42–45 wt %). Two types of trace-element patterns were found in the Schirmacher Hills: one is low to moderate K, Rb and Ba enrichment (e.g. S4, S6 and S8 in

Table 2. Selected whole-rock compositions of the mafic gneisses and granulites in central DML

Sample no.	0802 0402	0802 0404B	0802 0404D	0802 0406A	0112 1902A	B0112 2102A	B0112 2109	0201 0301J	0201 0602B
ID no.	S3	S4	S5	S6	H4	H7	H8	F9	F20
XRF analysis									
SiO ₂	45.83	49.80	48.25	47.00	48.91	50.21	46.47	47.57	49.34
TiO ₂	2.39	1.95	0.91	2.16	0.77	1.29	1.36	0.76	1.04
Al ₂ O ₃	13.71	15.44	13.88	13.85	15.27	15.07	14.28	13.42	13.30
Fe ₂ O ₃	15.63	11.92	18.72	15.51	9.90	12.14	12.71	11.52	11.06
MnO	0.23	0.15	0.24	0.24	0.16	0.18	0.19	0.21	0.18
MgO	7.32	7.64	9.49	7.46	8.62	7.74	8.58	12.52	11.67
CaO	11.38	8.70	4.30	11.39	10.31	11.78	12.34	7.11	7.32
Na ₂ O	1.77	2.84	1.92	1.76	3.55	0.54	1.00	2.18	2.16
K ₂ O	1.21	0.94	2.06	0.38	1.09	0.09	0.39	2.11	2.91
P ₂ O ₅	0.25	0.38	0.11	0.20	0.14	0.11	0.11	0.09	0.19
Total	99.71	99.77	99.88	99.95	98.73	99.15	97.44	97.49	99.57
Ba	95	142	438	63	92	37	27	152	586.1
Co	49	56	49	48	45	55	50	55	40
Cr	289	305	1197	220	394	236	395	1217	772
Nb	7.6	17.6	10.5	6.9	3.2	3.2	2.4	2.5	5.5
Ni	93	234	185	74	170	103	153	336	192.4
Rb	48.9	17.7	93.8	10.5	32.4	3.3	9.2	171.2	346.8
Sr	87	453	70	94	254	70	57	112	364.9
V	406	176	247	397	189	296	304	186	169.3
Y	40	21.6	17.4	37.2	20.3	32.3	30.1	7.0	21.1
Zr	153	185	90	121	94	88	91	68	102.8
INAA analysis									
Sc (0.1)*	52.8	21.5	43.1	54.4	33.4	51.8	47.0	32.6	29.8
ICP-MS analysis									
V (5)	426	180	247	416	197	308	311	185	167
Cr (20)	297	315	1170	225	441	261	432	1350	702
Co (1)	53	54	47	52	47	56	52	53	53
Ni (20)	70	200	180	60	150	90	120	270	210
Cu (10)	40	30	<10	60	20	10	20	<10	<10
Zn (30)	140	140	200	160	110	120	100	210	150
Ga (1)	23	25	26	23	18	22	19	21	20
Ge (0.5)	2.3	2.0	3.0	2.4	1.9	3.4	2.1	3.2	2.7
Rb (1)	55	15	112	6	31	<1	6	181	357
Sr (2)	87	437	69	96	232	64	51	100	368
Y (0.5)	51.8	21.8	23.1	44.9	19.8	33.9	31.3	13.6	20.1
Zr (1)	163	192	89	126	86	80	73	54	137
Nb (0.2)	5.2	16.7	6.7	4.2	3.4	3.2	1.8	3.5	5.4
Cs (0.1)	4.1	0.4	3.7	<0.1	1.0	<0.1	0.1	65.9	35.6
Ba (3)	94	149	389	42	68	12	12	136	707
La (0.05)	8.65	20.6	9.68	7.20	11.7	5.78	3.81	4.83	13.6

(Continued)

Table 2. (Continued)

Sample no.	0802 0402	0802 0404B	0802 0404D	0802 0406A	0112 1902A	B0112 2102A	B0112 2109	0201 0301J	0201 0602B
ID no.	S3	S4	S5	S6	H4	H7	H8	F9	F20
Ce (0.05)	23.7	47.1	20.2	20.5	25.5	15.1	10.4	10.7	31
Pr (0.01)	3.71	6.18	2.63	3.35	3.16	2.28	1.68	1.49	4.09
Nd (0.05)	18.9	26.9	11.2	16.8	13.3	11.1	8.64	6.75	17.3
Sm (0.01)	6.07	6.51	2.93	5.39	3.22	3.86	3.09	2.01	4.05
Eu (0.005)	2.04	2.03	1.01	1.80	1.05	1.20	1.06	0.682	1.51
Gd (0.01)	7.89	6.15	3.50	7.05	3.38	5.11	4.36	2.18	3.86
Tb (0.01)	1.47	0.91	0.64	1.32	0.58	0.98	0.86	0.39	0.64
Dy (0.01)	9.22	4.51	4.05	8.14	3.39	6.07	5.27	2.44	3.66
Ho (0.01)	1.81	0.77	0.82	1.59	0.66	1.20	1.10	0.50	0.70
Er (0.01)	5.30	1.95	2.43	4.68	1.93	3.53	3.31	1.45	1.99
Tm (0.005)	0.796	0.262	0.365	0.691	0.280	0.511	0.493	0.214	0.288
Yb (0.01)	5.27	1.65	2.47	4.59	1.86	3.42	3.27	1.42	1.96
Lu (0.002)	0.882	0.269	0.412	0.749	0.311	0.556	0.535	0.238	0.322
Hf (0.1)	3.8	4.1	2.0	3.0	2.0	2.2	1.9	1.3	3.1
Ta (0.01)	0.29	1.09	0.34	0.26	0.22	0.37	0.14	0.22	0.38
W (0.5)	<0.5	0.8	<0.5	<0.5	<0.5	<0.5	0.6	0.7	0.6
Tl (0.05)	0.28	0.07	0.51	0.05	0.23	<0.05	0.05	1.25	2.45
Pb (5)	<5	<5	5	<5	12	<5	<5	7	6
Th (0.05)	0.91	1.73	0.36	1.19	2.17	0.54	0.38	0.63	0.88
U (0.01)	0.34	0.65	0.19	0.48	2.19	4.00	0.76	0.99	0.68

Fe as Fe₂O₃. Detection limit of ICP-MS is listed in parentheses.

Fig. 5a), and the other is high enrichment (S2, S3 and S5 in Fig. 5b). Both types showed a flat pattern or slight decrease from Nb to Y. Some samples displayed negative P and Ti anomalies (Fig. 5b). Trace-element patterns for the mafic to ultramafic rocks from Filchnerfjella are characterized by high large ion lithophile element (LILE) (K, Rb and Ba) enrichment and a flat to slight decrease in the high-field-strength elements (HFSEs) (Fig. 5d, e). Low abundances of HFSEs compared to N-MORB (Fig. 5d) were observed in some Filchnerfjella samples. Except for the ultramafic rock, these patterns resemble island arc and continental arc basalts (Fig. 5h, k). Hochlinfjellet and Jutulsessen had similar abundance patterns (Fig. 5c, f). The trace elements in H4, H7 and H8 are almost identical to N-MORB with respect to the Nb to Y contents (Fig. 5c).

The REE pattern (Fig. 6a) for the rocks from the Schirmacher Hills can be divided into several groups: (1) almost flat (S3, S6, S8 and S9), (2) depleted from light REEs (LREEs) to heavy REEs (HREEs), parallel to the enriched MORB (E-MORB) pattern (S5 and S4), and (3) those with negative Eu anomalies (S1 and S2). The rocks from Hochlinfjellet (H7 and H8) and Jutulsessen (T4) showed an almost flat pattern (Fig. 6b, c). Samples from Filchnerfjella are characterized by moderate to high enrichment in LREEs and depletion in HREEs (Fig. 6d, e). Several samples preserved both negative and positive Eu anomalies.

6. Discussion

6.a. Precursors of the mafic gneisses/granulites

We selected the samples likely to have preserved primitive basaltic compositions based on the Mg number versus SiO₂/Al₂O₃ diagram (Fig. 4). Suda *et al.* (2008) conducted the same selection and reported reliable results even for the high-grade gneisses. The majority of the compositions of the analysed samples plotted either around the compositional field of 'primitive' basaltic magmas or corresponded to the tholeiitic fractionation trend. We selected the samples within the dashed circle in the first step here.

Metamorphic rocks, especially high-temperature metamorphic rocks, are considered to undergo various element transport processes caused by a metamorphic differentiation, partial melting and dehydration with increasing metamorphic grade. In the second step, samples with abnormal REE contents, particularly Eu anomalies, were excluded to eliminate the uncertain effects mentioned above. For example, the negative Eu anomaly is presumably influenced by plagioclase-bearing melt loss during high-grade metamorphism. The negligibly affected samples were S3, S4, S5, S6, H4, H7, H8, F6, F7, F9 and F20. Considering those with a SiO₂ content in the range of 45–52 wt %, these sample compositions were plotted in several discrimination diagrams to determine the tectonic setting of the precursor mafic rocks.

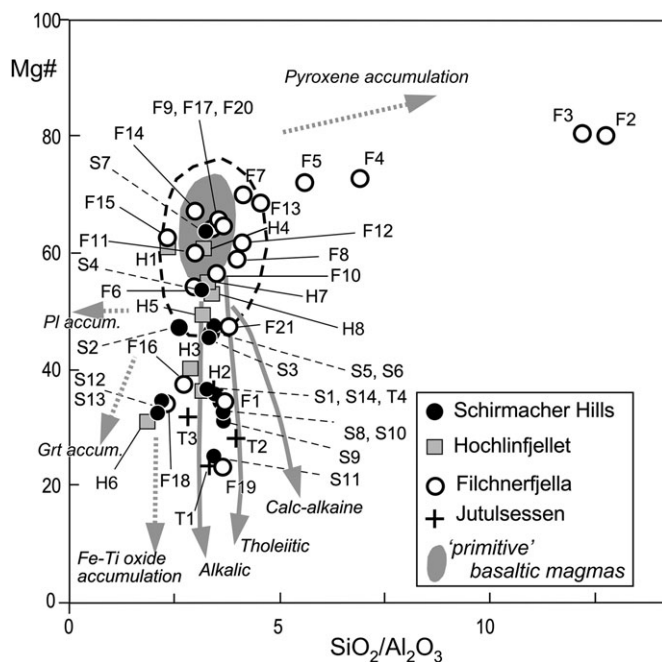


Fig. 4. Mg number versus $\text{SiO}_2/\text{Al}_2\text{O}_3$ diagram for the mafic granulite/gneiss. The grey field represents 'primitive' basaltic magmas; grey arrows show differentiation trends of tholeiite and calc-alkaline. The dashed grey arrows showing the generalized direction of compositional change with accumulation of the indicated mineral phases are from Kempton & Harmon (1992) and Kempton *et al.* (1997). Data plotted inside of the dashed circle were used for discrimination.

Figure 7a, b shows the Zr–Nb–Y diagram (Meschede, 1986) and La–Nb–Y diagram (Cabanis & Lecolle, 1989). The analysed samples plotted in a wide range of fields in both diagrams. The Schirmacher Hills samples were seen as a continuous trend through within-plate basalt (WPB), volcanic arc and N-MORB (Fig. 7a), similar to the HFSE depletion of the Northeast Japan arc (Shuto *et al.* 1995). Other samples from Hochlinfjellet (H7 and H8) plotted in similar fields to samples S3 and S6, but sample H4 was slightly different. Samples F6, F7, F20 and H4 plotted in the field of calc-alkali basalts in Figure 7b. In Figure 7b, samples S3, S6, H7 and H8 plotted in the narrow 2B field, representing back-arc basin basalt (less well defined). Other data plotted in the fields of continental basalts.

Figure 8 shows the Th/Yb–Nb/Yb diagram (Pearce, 2008), which discriminates between rocks enriched by subduction, crustal contamination and deep crustal recycling. The fields of the different localities of basaltic rocks are shown. The field for the Mariana Trough representing a back-arc setting was obtained from Pearce (2008). Pearce (2008) noted that 'Back-arc basin basalts (BABB) may lie within the MORB–OIB array if the subduction component does not influence the inflowing mantle. However, the compositions were displaced from the MORB–OIB array.' The data for the mafic gneisses from the Schirmacher Hills plotted over a wide range. Samples S4 and S5 plotted within the mid-ocean ridge – ocean island basalt (MORB–OIB) array fields. Other data for S3 and S6 plotted in the field of the Mariana Trough basalts together with those of H7 and H8. The field represents BABB, and the plotted data were identical, with a slight increase in arc proximity, as in the above note from Pearce (2008). Sample H4 displayed a high Th/Yb ratio and plotted in the field of arc basalt. Two samples from Filchnerfjella plotted in a narrow range of $\text{Th}/\text{Yb} = 0.4$ and $\text{Nb}/\text{Yb} = 2.5$. Additional data with slight Eu anomalies (F11 and

F13, represented by a grey circle in Fig. 8) plotted in the field of the Mariana and Kamchatka arcs.

The REE patterns of the selected samples are shown in Figure 9. Samples from the Schirmacher Hills display different patterns: almost flat (S3 and S6), and slightly and highly depleted from LREEs to HREEs (S5 and S4). The REE patterns of samples S4 and S5 are almost parallel to those of the within-plate basalts (WPB, OIB and WPA) and E-MORB, respectively. Similar flat REE patterns of S3 and S6 can be seen in samples H7 and H8 from Hochlinfjellet, respectively. H7 and H8 contain REE abundances between N-MORB and BABB. Samples S3 and S6 were slightly enriched in HREEs compared to that of BABB. Another sample, H4, resembled that of S4. Two samples from Filchnerfjella were almost parallel to island arc basalt (IAB) (F9) and within-plate tholeiite (WPT) (F20). Table 3 summarizes the possible tectonic settings of the protoliths according to the above discrimination.

6.b. Tectonic setting and timing

Figure 10 shows a concordant age histogram of the three localities in central DML based on the U–Pb ages published by Baba *et al.* (2010, 2015). Ravikant *et al.* (2018) and Elvevold *et al.* (2020) reported U–Pb zircon age data obtained by laser-ICP-MS and isotope dilution thermal ionization mass spectrometry (ID-TIMS) in the Schirmacher Hills and Hochlinfjellet, although they ignored the internal texture of zircon concerning the metamorphic event, resulting in uncertainty. We referred to reliable data obtained by spot analyses to consider the zircon internal domain (Jacobs *et al.* 2003, 2020).

6.b.1. Schirmacher Hills

Metamorphism involving UHT and tectonothermal events in the Schirmacher Hills pre-dates other inland nunataks. Based on the geochemical results of Rameshwar Rao *et al.* (2000), Baba *et al.* (2010) proposed that the c. 650 Ma UHT metamorphic event in the Schirmacher Hills occurred in a back-arc tectonic setting and pre-dated the main collisional event of central DML (c. 550–500 Ma).

Shuto *et al.* (1995) reported that basaltic rocks exposed along the Japanese Sea exhibit geochemical variation. As with the opening of the Japanese Sea, within the development of the back-arc basin, basaltic rock compositions vary from an HFSE-enriched OIB source to an N-MORB source to a highly incompatible HFSE-depleted IAB source (dashed line in Fig. 7a), with decreasing age. Our data show that the geochemical compositions of the mafic gneiss/granulites from the Schirmacher Hills are comparable with WPB/OIB to N-MORB (Fig. 7a), and the trace-element patterns resemble those of the basaltic rocks in the current back-arc setting (Japanese Sea: Mishima, E-Scotia in Fig. 5). A back-arc setting for the mafic rock in the Schirmacher Hills is most likely based on the other discrimination diagrams (see Table 3); therefore, the previous inference of Baba *et al.* (2010) is confirmed.

The oscillatory zircon concordant core age from the felsic gneiss (e.g. Hbl-Bt in Fig. 10) and the granitic gneiss in the Schirmacher Hills and adjacent nunatak was c. 800 Ma (Baba *et al.* 2010; Jacobs *et al.* 2020). The main protoliths for these basement rocks were formed by magmatism at c. 800 Ma. Jacobs *et al.* (2020) proposed that a possible tectonic setting for these basement rocks is an active continental margin setting. However, older zircon ages (>1000 Ma) expected to be derived from a pre-existing older continental origin are lacking (see Fig. 10); hence, a juvenile arc or oceanic arc setting are likely to be alternative settings.

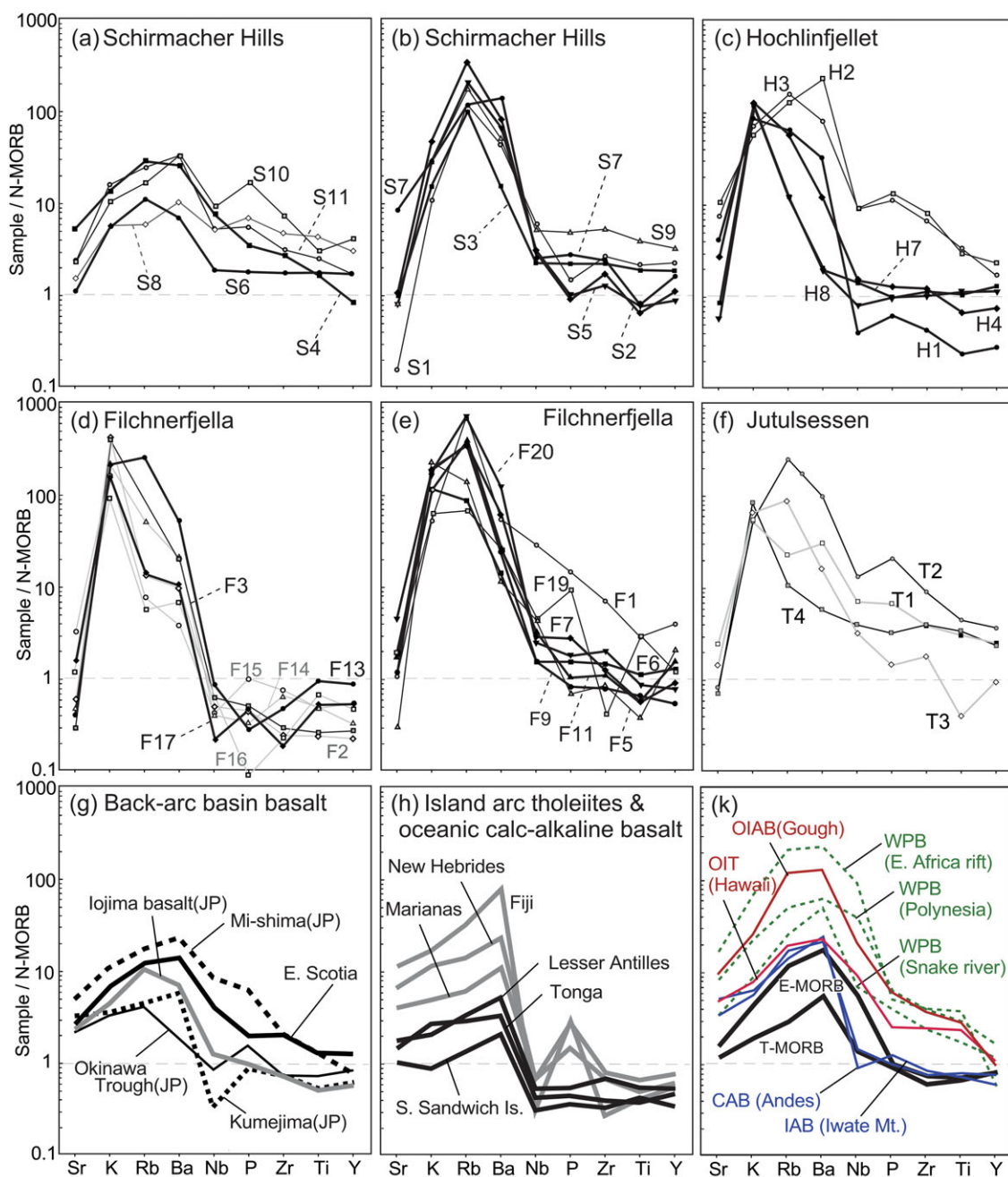


Fig. 5. (Colour online) N-MORB-normalized trace-element concentrations in the mafic granulite/gneiss. (a–f) This study. (g, h, k) References for basaltic rock in various tectonic settings. Data for Iojima (Japan: JP), Okinawa Trough (JP), Mi-shima (JP) and Kume-jima (JP) are taken from Ito & Shiraki (1999) and references therein. E. Scotia is taken from Saunders & Tarney (1979). Abbreviations: CAB – continental arc basalt; E-MORB – enriched mid-ocean ridge basalt; IAB – island arc basalt; OIB – oceanic island basalt; OIAB – oceanic island alkali basalt; OIT – oceanic island tholeiite; T-MORB – transitional mid-ocean ridge basalt; WPB – within-plate basalt. Normalization factors from Sun & McDonough (1989).

The mafic gneisses analysed here occur as layers and discontinuous blocks. Their timing of emplacement could not be determined owing to subsequent deformation. The analysed samples preserve compositions similar to primary magmatic compositions (Fig. 4) and display minor Eu anomalies, suggesting that they did not suffer significant metamorphic disturbance. We assume that they were emplaced close to the metamorphic peak (*c.* 650 Ma) in a back-arc setting.

6.b.2. Hochlinfjellet

The geochemical compositions of the two mafic gneisses (H7 and H8) from Hochlinfjellet are similar to those of the Schirmacher Hills. They are assumed to be derived from magmatism in the same tectonic setting. These mafic gneisses were collected from the same locality where the metasedimentary rocks record metamorphic ages of 630 Ma and 600 Ma (Baba *et al.* 2015). Sample B01122102B contains oscillatory zoned zircons with ages of

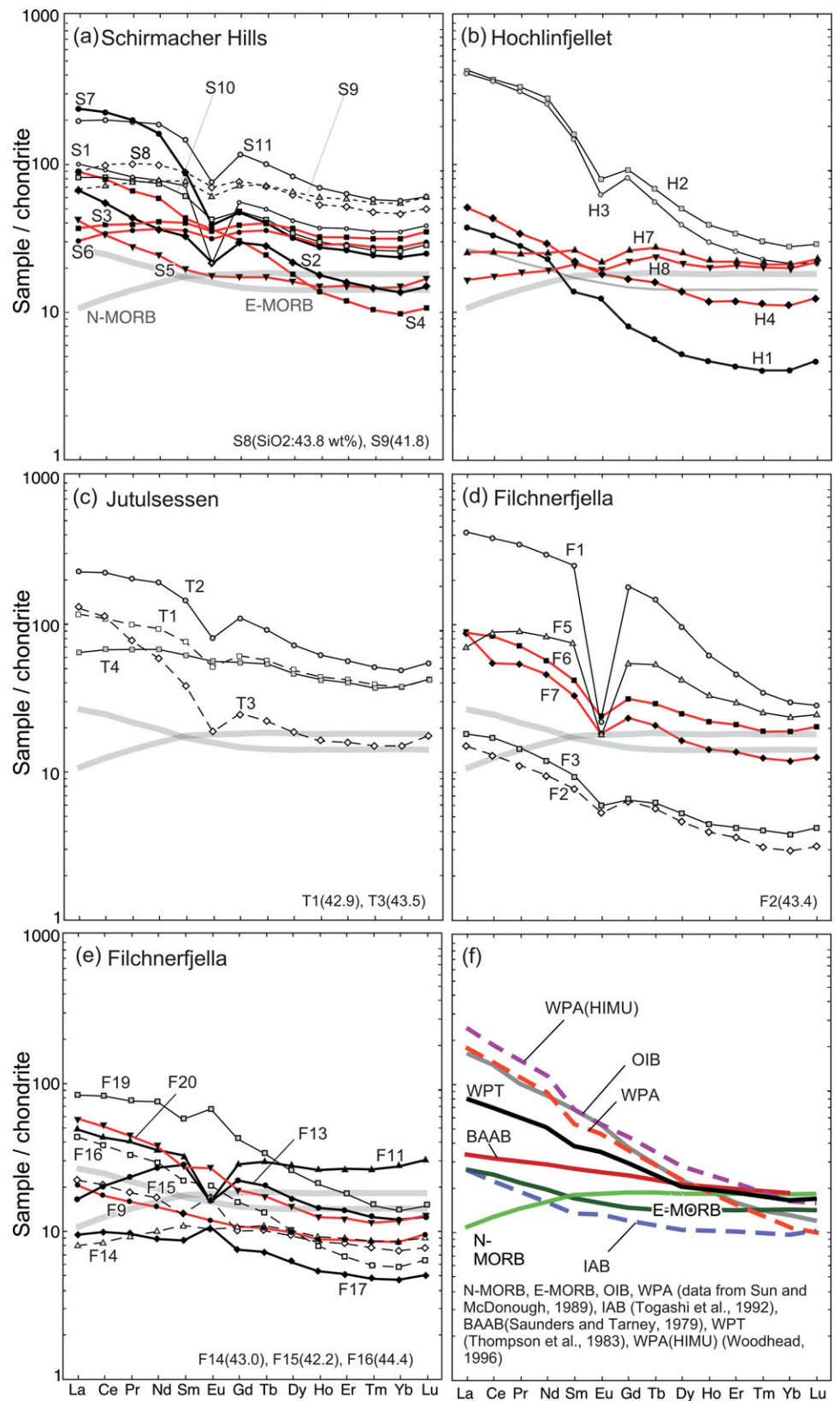


Fig. 6. (Colour online) Chondrite-normalized REE patterns. (a–e) This study. (f) Reference data for normal mid-ocean ridge basalt (N-MORB), enriched mid-ocean ridge basalt (E-MORB), oceanic island basalt (OIB) and within-plate alkali basalt (WPA) from Sun & McDonough (1989), island arc basalt (IAB) from Togashi *et al.* (1992), back-arc basin basalt (BAAB) from Saunders & Tarney (1979), within-plate tholeiite (WPT) from Thompson *et al.* (1983) and WPA (HIMU) from Woodhead (1996). Solid lines represent data plotted inside of the dashed circle in Figure 4. Dashed line is data with a low SiO₂ content of between 45 and 42 wt%. Red lines are the data used for the discrimination plots.

c. 1.2 Ga, 0.9 Ga and 0.8 Ga, but these older age grains are sparse. Therefore, the contribution of a continental component to the protoliths of the basement rocks is limited. Samples H7 and H8 were collected from the central part of Hochlinfjellet (Fig. 1b), but

sample H4 from the southern part has an IAB signature. This geochemical difference is correlated with the differences in metamorphic ages. Jacobs *et al.* (2003) reported that a basement rock in an inland nunatak of Hochlinfjellet has metamorphic ages of 558 Ma

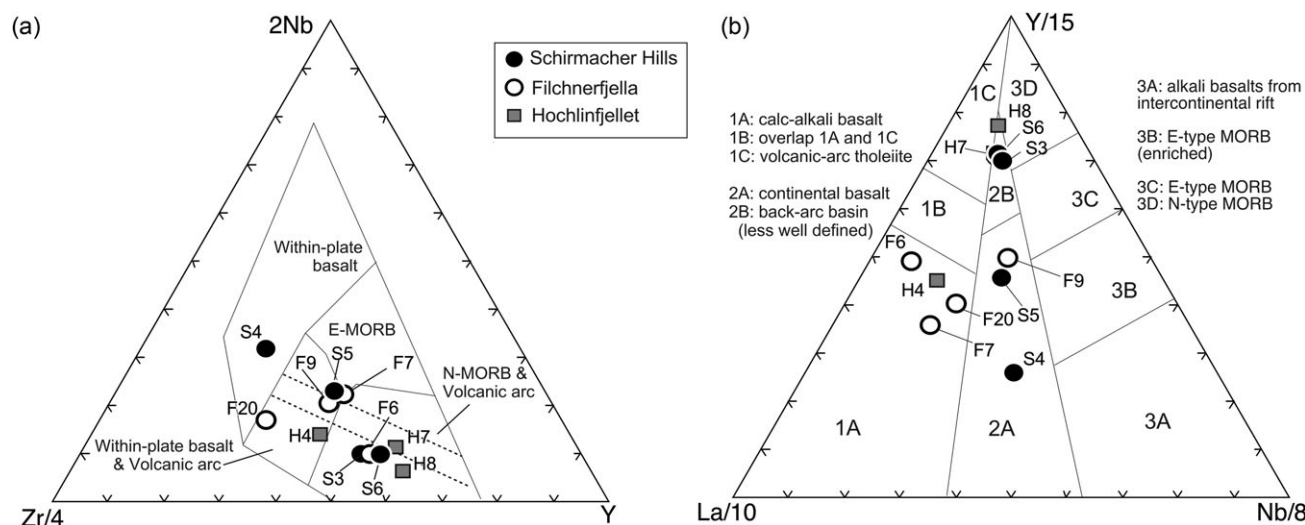


Fig. 7. Discrimination plots for the selected mafic gneiss/granulite data based on Figures 5, 6 and 7 (see text). (a) Zr–Y–Nb discrimination diagram (Meschede, 1986) for the mafic rocks. Dashed line shows HFSE depletion trend of the Northeast Japan arc (Shuto *et al.* 1995). (b) La–Nb–Y discrimination diagram (Cabaniš & Lecolle, 1989). MORB – mid-ocean ridge basalt.

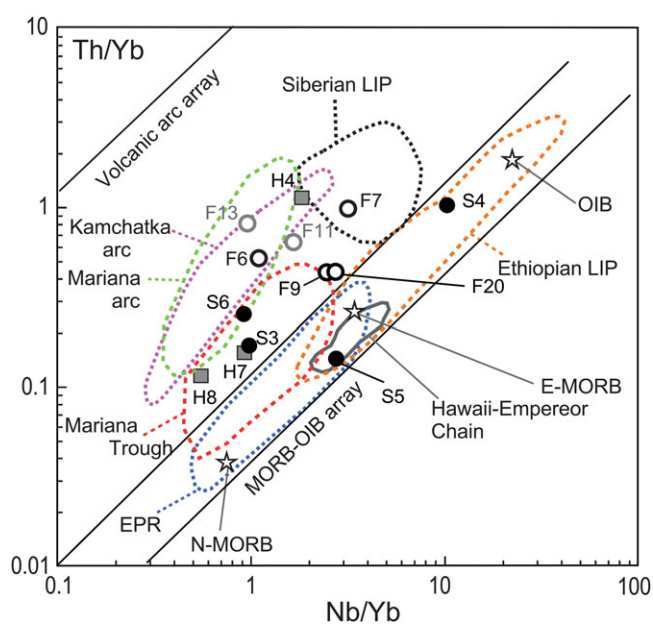


Fig. 8. (Colour online) Th/Yb versus Nb/Yb discrimination diagram (modified after Pearce, 2008). The fields for the Siberian large igneous province (LIP) (from Desta *et al.* 2015 and references therein); Ethiopian LIP (Beccaluva *et al.* 2009); Kamchatka arc (Churikova *et al.* 2001); Mariana arc and Mariana Trough (Pearce, 2008); East Pacific Rise (EPR) (Turner *et al.* 2011); and Hawaiian–Emperor Chain (Huang *et al.* 2005) are shown for comparison. N-MORB, E-MORB and OIB are from Sun & McDonough (1989).

and 530–520 Ma. Based on the difference in metamorphic age compared to the central part (630–600 Ma), Baba *et al.* (2015) proposed a possible terrane boundary between them (see line A, Figs 1b, 2b). This terrane boundary is supported by the geochemical differences in the mafic gneisses.

6.b.3. Filchnerfjella

Most of the mafic gneisses in Filchnerfjella showed distinctive Eu anomalies and did not preserve the primary magmatic compositions (Figs 4, 6). The compositions may suggest element mobilization by addition or extraction of partial melt and metamorphic

differentiation during the prograde stage. The unaffected samples (F9 and F20) have geochemical affinities with continental or island arc basalt (Table 3). The meta-sediment (02010502E) in the layered gneiss unit (Fig. 2d) contains zircon grains with ages of c. 1800–1700 Ma, 1200 Ma, 950 Ma and 650 Ma (Fig. 10). The protolith of the metasedimentary rock was derived from a mature continental component. The metamorphic ages are well concentrated from 530 to 520 Ma, and the youngest detrital zircon of c. 650 Ma is present (Baba *et al.* 2015). At the peak metamorphism of the Schirmacher Hills and Hochlinfjellet, the metasedimentary protolith for Filchnerfjella is considered to be the final depositional stage in a continental arc setting. Sample 02010201B is an orthopyroxene-bearing homogeneous gneiss in the brown gneiss unit that possibly originated from c. 1100 Ma igneous rocks. The timing of the emplacement of the mafic protolith is not well constrained. However, we can assume that (1) it was formed coeval with the c. 1100 Ma igneous activity and intruded into felsic igneous rocks in a continental arc, or (2) it was emplaced into the sedimentary rocks at the subduction zone in a marginal continental arc. Samples F9 and F20 were collected from the leucogneiss unit. Similar geochemical patterns were obtained for samples F6, F7, F11 and F13 in the layered gneiss unit (Fig. 2), which involves voluminous layered mafic gneiss (Owada *et al.* 2003). Combining the wide range of U–Pb ages for the detrital zircons in sample 02010502E from the layered gneiss unit with the disturbed geochemical signature of the mafic gneiss implies repeated magmatic events. They occurred in a continental arc setting to form mafic gneiss protoliths and have continued for a long time. Filchnerfjella lacks an 800 Ma zircon population and has a different geochemical affinity than that of the Schirmacher Hills, implying that they formed in a different geological setting and with different timing.

7. Conclusion

Precursors for the mafic gneiss and granulite in central DML were formed in different geological backgrounds and tectonic settings. The mafic gneisses and granulites from the Schirmacher Hills were derived from basaltic rocks extruded in a back-arc setting. From the perspective of the protolith ages of the basement rocks and

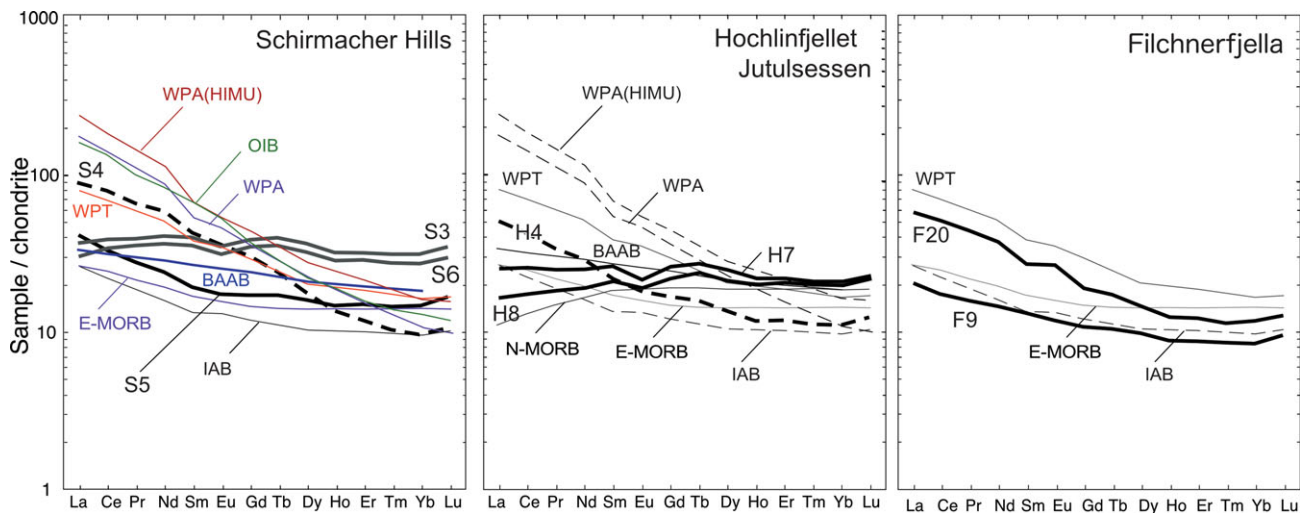


Fig. 9. (Colour online) Chondrite-normalized REE patterns of the selected samples. Reference data and abbreviations are as in Figure 6.

Table 3. Summary of inferred tectonic setting using different discrimination diagrams

Sample no.	Id no.	Occurrences	SiO ₂	Possible setting	ICP-MS Nb–Zr–Y diagram	ICP-MS Y–La–Nb diagram	ICP-MS Nb/Yb–Th/Yb	ICP-MS chondrite pattern	ICP-MS + XRF MORB normalized	Note
08020402	S3	In felsic layer	45.83	BABB	N-MORB & VAB	BABB	BABB (Mariana)	Flat T-MORB	BABB	High REE
08020404B	S4	As layer in Grt-banded gneiss	49.80	OIB & WPB	WPB	Continental basalt	OIB (on array)	WPT	OIT & OIB	
08020404D	S5	As layer in Grt-banded gneiss	48.25	WPB	WPB & VAB	Continental basalt	E-MORB (Hawaii on array)	E-MORB	IAT & CAB	
08020406A	S6	As block in felsic gneiss	47.00	BABB	N-MORB & VAB	BABB	BABB (Mariana)	Flat T-MORB	BABB	High REE
011221902A	H4	As layer in banded gneiss	48.91	IAB	WPB & VAB	Calc-alkali basalt	Arc	IAB-WPT	CAB & IAB	
B01122102A	H7	As layer in banded gneiss	50.21	BABB	N-MORB & VAB	BABB	BABB (Mariana)	T-MORB, BABB	N-MORB	
B01122109	H8	As block in felsic gneiss	46.47	BABB	N-MORB & VAB	BABB	BABB (Mariana)	N-MORB	N-MORB	
02010202J	F6	As layer in banded gneiss	47.45	CAB or IAB	N-MORB & VAB	Calc-alkali basalt	Arc	WPT	CAB & IAB	High HREE
02010203B	F7	As layer in banded gneiss	48.97	CAB or IAB	N-MORB & VAB	Calc-alkali basalt	Arc	WPT	–	
02010301J	F9	As enclave in Grt-gneiss	47.57	CAB or IAB	WPB & VAB	Continental basalt	Arc	IAB	IAT & CAB	
02010602 B	F20	As block in leucogneiss	49.34	CAB or IAB	WPB & VAB	Calc-alkali basalt	Arc	WPT	IAT & CAB	

BABB – back arc basin basalt; OIB – oceanic island basalt; WPB – within-plate basalt; IAB – island arc basalt; CAB – continental arc basalt; VAB – volcanic arc basalt; WPT – within-plate tholeiite; OIT – oceanic island tholeiite; WPA – within-plate alkali basalt; IAT – island arc tholeiite; E-MORB – enriched mid-ocean ridge basalt; N-MORB – normal mid-ocean ridge basalt; T-MORB – transitional mid-ocean ridge basalt; Grt – garnet; REE – rare earth elements.

geochemical variation, they were emplaced during 800–650 Ma, close to the peak metamorphism without metamorphic differentiation and partial melting that could have occurred during the prograde stage. Similar protoliths were recognized in inland nunataks of Hochlinfjellet. In Filchnerfjella, mafic gneisses/granulites were derived from basaltic rocks formed in marginal continental arcs or island arcs. However, metamorphic processes influenced their

geochemical composition during the prograde metamorphic stage. Our results imply that the outcrops in central DML with different metamorphic ages contain mafic gneisses/granulites derived from precursor rocks formed in different tectonic settings. This geological background supports the preliminary terrane division of Baba *et al.* (2015). Furthermore, the principle concept supports the tectonic model of Jacobs *et al.* (2020), which involves separate

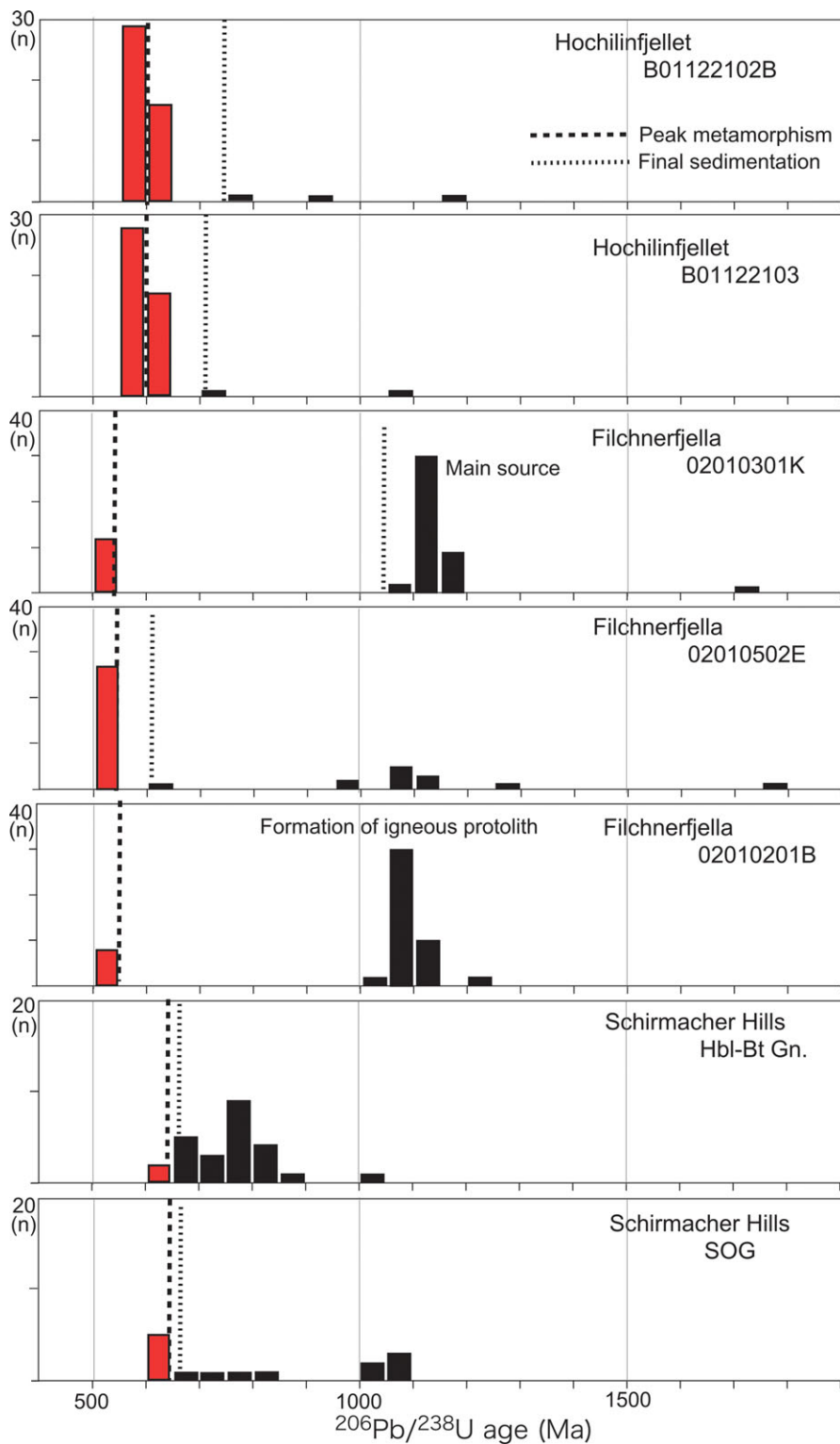


Fig. 10. (Colour online) Age histograms of the zircon concordia ages from three localities in central DML. Data are taken from Baba *et al.* (2010, 2015).

tectonothermal events between the Schirmacher Hills and inland nunataks.

Supplementary material. To view supplementary material for this article, please visit <https://doi.org/10.1017/S0016756823000092>.

Acknowledgements. We thank Y. Osanai and T. Toyoshima for giving us an opportunity to re-visit the Schirmacher Hills during the 49th Japanese Antarctic Expedition at the Sør Rondane Mountains and K. Shiraishi for the arrangement of the Norway–Germany–Japan joint expedition 2001–2002. S. Elvevold and A. Läufer are grateful for their collaboration in the fieldwork during the joint

expedition in the inland nunatak of central DML. SB acknowledges R. Shinjo, H. Matsushita and N. Miyagi for their support with XRF analyses at the University of the Ryukyus. We thank anonymous reviewers for constructive comments, and T. Johnson for editorial handling. This work was partly supported by the National Institute of Polar Research [General Collaboration Projects 25–17 and 2–20], the Research Organization of Information and Systems [ROIS-DS-JOINT 004RP2018] and the Japan Society for the Promotion of Science (JSPS) [15K05346 to SB].

Conflicts of interest. None.

References

- Baba S, Hokada T, Kaiden H, Dunkley DJ, Owada M and Shiraishi K (2010) SHRIMP zircon U-Pb dating of sapphirine-bearing granulite and biotite-hornblende gneiss in the Schirmacher Hills, east Antarctica: implications for Neoproterozoic ultrahigh-temperature metamorphism predating the assembly of Gondwana. *Journal of Geology* **118**, 621–39.
- Baba S, Horie K, Hokada T, Owada M, Adachi T and Shiraishi K (2015) Multiple collisions in the east African-Antarctica orogen: constraints from timing of metamorphism in the Filchnerfjella and Hochlinfjellet terranes in central Dronning Maud Land. *Journal of Geology* **123**, 55–75.
- Baba S, Owada M, Grew ES and Shiraishi K (2006) Sapphirine granulite from Schirmacher Hills, central Dronning Maud Land. In *Antarctic Contributions to Global Earth Science* (eds DK Fütterer, D Damaske, G Kleinschmidt, H Miller and F Tessensohn), pp. 37–44. Berlin: Springer.
- Baba S, Owada M and Shiraishi K (2008) Contrasting metamorphic P-T path between Schirmacher Hills and Mühlig-Hofmannfjella, central Dronning Maud Land, East Antarctica. In *Geodynamic Evolution of East Antarctica: A Key to the East–West Gondwana Connection* (eds M Satish-Kumar, Y Motoyoshi, Y Osani, Y Hiroi and K Shiraishi), pp. 401–17. Geological Society of London, Special Publication no. 308.
- Beccaluva L, Bianchini G, Natali C and Siena F (2009) Continental flood basalts and mantle plumes: a case study of the northern Ethiopian Plateau. *Journal of Petrology* **50**, 1377–403.
- Bingen B, Jacobs J, Viola G, Hendersson IHC, Skår Ø, Boyd R, Thomas RJ, Solli A, Key RM and Daudi EXF (2009) Geochronology of the Precambrian crust in the Mozambique belt in NE Mozambique, and implications for Gondwana assembly. *Precambrian Research* **170**, 231–55.
- Bucher K and Frost BR (2006) Fluid transfer in high-grade metamorphic terranes intruded by anorogenic granites: the Thor Range, Antarctica. *Journal of Petrology* **47**, 567–93.
- Cabanis B and Lecolle M (1989) Le diagramme La/10-Y/15-Nb/8: un outil pour la discrimination des series volcaniques et la mise en evidence des processus de melange et/ou de contamination crustale. *Comptes Rendus de l'Academie des Sciences, Serie 2* **309**, 2023–9.
- Churikova T, Dorendorf F and Worner G (2001) Sources and fluids in the mantle wedge below Kamchatka, evidence from across-arc geochemical variation. *Journal of Petrology* **42**, 1567–93.
- Desta MT, Ishiwatari A, Sumiaki Machi S, Arai S, Tamura A, Ledneva GV, Sokolov SD, Moiseev AV and Bazylev BA (2015) Petrogenesis of Triassic gabbroic and basaltic rocks from Chukotka, NE Russia: eastern end of the 'arc-type' Siberian LIP? *Journal of Mineralogical and Petrological Sciences* **110**, 249–75.
- Elvevold S, Engvik AK, Abu-Alam, TS, Myhre PI and Corfu F (2020) Prolonged high-grade metamorphism of supracrustal gneisses from Mühlig-Hofmannfjella, central Dronning Maud Land (East Antarctica). *Precambrian Research* **339**, 105618. doi: [10.1016/j.precamres.2020.105618](https://doi.org/10.1016/j.precamres.2020.105618).
- Engvik AK and Elvevold S (2004) Pan-African extension and near-isothermal exhumation of a granulite facies terrain, Dronning Maud Land, Antarctica. *Geological Magazine* **141**, 649–60.
- Fitzsimons ICW (2000) Grenville-age basement provinces in East Antarctica: evidence for three separate collisional orogens. *Geology* **28**, 879–82.
- Grantham GH, Macey PH, Horie K, Kawakami T, Ishikawa M, Satish-Kumar M, Tsuchiya N, Graser P and Azevedo S (2013) Comparison of the metamorphic history of the Monapo Complex, northern Mozambique and Balchenfjella and Austhameren area, Sør Rondane, Antarctica: implications for the Kuunga Orogeny and the amalgamation of N and S. Gondwana. *Precambrian Research* **234**, 85–135.
- Grantham GH, Macey PH, Ingram BA, Roberts MP, Armstrong RA, Hokada T, Shiraishi K, Jackson C, Bisnath A and Manhica V (2008) Terrane correlation between Antarctica, Mozambique and Sri Lanka; comparisons of geochronology, lithology, structure and metamorphism and possible implications for the geology of south Africa and Antarctica. In *Geodynamic Evolution of East Antarctica: A Key to the East–West Gondwana Connection* (eds M Satish-Kumar, Y Motoyoshi, Y Osani, Y Hiroi and K Shiraishi), pp. 85–119. Geological Society of London, Special Publication no. 308.
- Huang S, Regelous M, Thordarson T and Frey FA (2005) Petrogenesis of lavas from Detroit Seamount: geochemical differences between Emperor Chain and Hawaiian volcanoes. *Geochemistry, Geophysics, Geosystems* **6**, Q01L06. doi: [10.1029/2004GC000756](https://doi.org/10.1029/2004GC000756).
- Ito J and Shiraki K (1999) Picrite basalts from the Pliocene Ueguskudake Formation in Kume-jima, Ryukyu Island. *Journal of the Geological Society of Japan* **105**, 810–13.
- Jacobs J, Bauer W and Fanning CM (2003) Late Neoproterozoic/Early Palaeozoic events in central Dronning Maud Land and significance for the southern extension of the East African Orogen into East Antarctica. *Precambrian Research* **126**, 27–53.
- Jacobs J, Elburg M, Läufer A, Kleinhanns IC, Henjes-Kunst F, Estrada S, Ruppel A, Damaske D, Montero P and Bea F (2015) Two distinct Late Mesoproterozoic/Early Neoproterozoic basement provinces in central-eastern Dronning Maud Land, East Antarctica: the missing link, 15–21E. *Precambrian Research* **265**, 249–72.
- Jacobs J, Mikhalsky E, Henjes-Kunst F, Läufer A, Thomas RJ, Elburg MA, Wang CC, Estrada S and Skublov S (2020) Neoproterozoic geodynamic evolution of easternmost Kalahari: constraints from U-Pb-Hf-O zircon, Sm-Nd isotope and geochemical data from the Schirmacher Oasis, East Antarctica. *Precambrian Research* **342**, 105553. doi: [10.1016/j.precamres.2019.105553](https://doi.org/10.1016/j.precamres.2019.105553).
- Jacobs J, Opås B, Elburg MA, Läufer A, Estrada S, Ksienzyk AK, Damaske D and Hofmann M (2017) Cryptic sub-ice geology revealed by a U-Pb zircon study of glacial till in Dronning Maud Land, East Antarctica. *Precambrian Research* **294**, 1–14.
- Jacobs J and Thomas RJ (2004) Himalayan-type indenter-escape tectonics model for the southern part of the late Neoproterozoic–early Paleozoic East African–Antarctic orogen. *Geology* **32**, 721–4.
- Kempton PD, Downes H and Embey-Isztin A (1997) Mafic granulite xenoliths in Neogene alkali basalts from the western Pannonian Basin: insights into the lower crust of a collapsed orogen. *Journal of Petrology* **38**, 941–70.
- Kempton PD and Harmon RS (1992) Oxygen isotope evidence for large-scale hybridization of the lower crust during magmatic underplating. *Geochimica et Cosmochimica Acta* **56**, 971–86.
- Meert J (2003) A synopsis of events related to the assembly of eastern Gondwana. *Tectonophysics* **362**, 1–40.
- Meschede M (1986) A method of discriminating between different types of mid-ocean ridge basalts and continental tholeiites with the Nb–Zr–Y diagram. *Chemical Geology* **56**, 207–18.
- Ohta Y (1993) Nature Environment Map, Gjelsvikfjella and Western Mühlig-Hofmannfjella, Dronning Maud Land, East Antarctica, Scale 1:100,000. Temakart 24. Norsk Polarinstittutt.
- Owada M, Baba S, Läufer A, Elvevold S, Shiraishi K and Jacobs J (2003) Geology of eastern Mühlig-Hofmannfjella and Filchnerfjella in Dronning Maud Land, East Antarctica: a preliminary report on a Japan–Norway–Germany joint geological investigation. *Polar Geosciences* **16**, 108–36.
- Owada M, Baba S, Osanai Y and Kagami H (2008) Geochemistry of post-kinematic mafic dykes from central to eastern Dronning Maud Land, East Antarctica: evidence for a Pan-African suture in Dronning Maud Land. In *Geodynamic Evolution of East Antarctica: A Key to the East–West Gondwana Connection* (eds M Satish-Kumar, Y Motoyoshi, Y Osani, Y Hiroi and K Shiraishi), pp. 235–52. Geological Society of London, Special Publication no. 308.
- Paulsson O and Austrheim H (2003) A geochronological and geochemical study of rocks from Gjelsvikfjella, Dronning Maud Land, Antarctica—

- implications for Mesoproterozoic correlations and assembly of Gondwana. *Precambrian Research* **125**, 113–38.
- Pearce JA** (2008) Geochemical fingerprinting of oceanic basalts with applications to ophiolite classification and the search for Archaean oceanic crust. *Lithos* **100**, 14–48.
- Rameshwar Rao D, Rashid SA and Panthulu GVC** (2000) Origin of Mg-metatholeiites of the Schirmacher region, East Antarctica: constraints from trace elements and Nd-Sr isotopic systematics. *Gondwana Research* **3**, 91–104.
- Rameshwar Rao D, Sharma R and Gururajan NS** (1997) Mafic granulites of Schirmacher region, East Antarctica: fluid inclusion and geothermobarometric studies focusing on the Proterozoic evolution of crust. *Transactions of the Royal Society of Edinburgh: Earth Sciences* **88**, 1–17.
- Ravikant V, Bühn B and Pimentel M** (2018) Zircon U-Pb age constraints for Tonian-early Cryogenian deposition of metasedimentary rocks from the Schirmacher Oasis, East Antarctica: implications for correlations across the Mozambique Ocean. *Polar Science* **18**, 39–47.
- Ruppel A, Jacobs J, Eagles G, Läufer A and Jokat W** (2018) New geophysical data from a key region in East Antarctica: estimates for the spatial extent of the Tonian Oceanic Arc Super Terrane (TOAST). *Gondwana Research* **59**, 97–107.
- Saunders AD and Tarney J** (1979) The geochemistry of basalts from a back-arc spreading centre in the East Scotia Sea. *Geochimica et Cosmochimica Acta* **43**, 555–72.
- Sengupta S** (1993) Tectonothermal history recorded in mafic dykes and enclaves of gneissic basement in the Schirmacher Hills, East Antarctica. *Precambrian Research* **63**, 273–91.
- Shinjo R and Miyamoto M** (2007) Analytical accuracy and precision of major and trace elements for bulk rocks using a 1:5 dilution glass bead by XRF. *Reports of the Faculty of Science of Ryukyu University* **84**, 5–13 (in Japanese with English abstract).
- Shiraishi K, Dunkley DJ, Hokada T, Fanning CM, Kagami H and Hamamoto T** (2008) Geochronological constraints on the Late Proterozoic to Cambrian crustal evolution of eastern Dronning Maud Land, East Antarctica: a synthesis of SHRIMP U-Pb age and Nd model age data. In *Geodynamic Evolution of East Antarctica: A Key to the East–West Gondwana Connection* (eds M Satish-Kumar, Y Motoyoshi, Y Osani, Y Hiroi and K Shiraishi), pp. 21–67. Geological Society of London, Special Publication no. 308.
- Shuto K, Nakajima S, Ohki J, Uematsu M, Watanabe N and Yamamoto K** (1995) High field strength element depletions in the lithospheric mantle beneath the Northeast Japan arc. *Memoir of the Geological Society of Japan* **44**, 241–62 (in Japanese with English abstract).
- Stern RJ** (1994) Arc assembly and continental collision in the Neoproterozoic East Africa Orogen: implications for the consolidation of Gondwana. *Annual Review of Earth and Planetary Sciences* **22**, 319–51.
- Suda Y, Kawano Y, Yaxley G, Korenaga H and Hiroi Y** (2008) Magmatic evolution and tectonic setting of metabasites from Lützow-Holm Complex, East Antarctica. In *Geodynamic Evolution of East Antarctica: A Key to the East–West Gondwana Connection* (eds M Satish-Kumar, Y Motoyoshi, Y Osani, Y Hiroi and K Shiraishi), pp. 211–33. Geological Society of London, Special Publication no. 308.
- Sun S-S and McDonough WF** (1989) Chemical and isotopic systematics of oceanic basalts: implications for mantle composition and processes. In *Magmatism in the Ocean Basins* (eds AD Saunders and MJ Norry), pp. 313–45. Geological Society of London, Special Publication no. 42.
- Thompson RN, Morrison MA, Dickin AP and Hendry GL** (1983) Continental flood basalts. . . Arachnids rule OK? In *Continental Basalts and Mantle Xenoliths* (eds CJ Hawkesworth and MJ Norry), pp. 158–85. Nantwich: Shiva.
- Togashi S, Tanak T, Yoshida T, Ishikawa K, Fujinawa A and Kurasawa H** (1992) Trace elements and Nd-Sr isotopes of arc tholeiites from frontal arc of Northeast Japan. *Geochemical Journal* **26**, 261–77.
- Turner S, Beier C, Niu Y and Cook C** (2011) U–Th–Ra disequilibria and the extent of off-axis volcanism across the East Pacific Rise at 9°30'N, 10°30'N, and 11°20'N. *Geochemistry, Geophysics, Geosystems* **12**, Q0AC12. doi: [10.1029/2010GC003403](https://doi.org/10.1029/2010GC003403).
- Woodhead JD** (1996) Extreme HIMU in an oceanic setting: the geochemistry of Mangaia Island (Polynesia), and temporal evolution of the Cook-Austral hotspot. *Journal of Volcanology and Geothermal Research* **72**, 1–19.